



LAWRENCE
LIVERMORE
NATIONAL
LABORATORY

An Analytic Model Of Thermal Drift In Piezoresistive Microcantilever Sensors

A. Loui, S. Elhadj, D. J. Sirbuly, S. K. McCall, B. R. Hart, T. V. Ratto

September 29, 2009

Journal of Applied Physics

Disclaimer

This document was prepared as an account of work sponsored by an agency of the United States government. Neither the United States government nor Lawrence Livermore National Security, LLC, nor any of their employees makes any warranty, expressed or implied, or assumes any legal liability or responsibility for the accuracy, completeness, or usefulness of any information, apparatus, product, or process disclosed, or represents that its use would not infringe privately owned rights. Reference herein to any specific commercial product, process, or service by trade name, trademark, manufacturer, or otherwise does not necessarily constitute or imply its endorsement, recommendation, or favoring by the United States government or Lawrence Livermore National Security, LLC. The views and opinions of authors expressed herein do not necessarily state or reflect those of the United States government or Lawrence Livermore National Security, LLC, and shall not be used for advertising or product endorsement purposes.

An analytic model of thermal drift in piezoresistive microcantilever sensors

A. Loui,^{a)} S. Elhadj, D.J. Sirbully, S.K. McCall, B.R. Hart, and T.V. Ratto

Lawrence Livermore National Laboratory, 7000 East Ave., Livermore, California 94550, USA

(Received

^{a)} Corresponding author. Tel.: +1 925 422-2840; fax: +1 925 422 3160

E-mail address: loui2@llnl.gov

ABSTRACT

A closed form semi-empirical model has been developed to understand the physical origins of thermal drift in piezoresistive microcantilever sensors. The two-component model describes both the effects of temperature-related bending and heat dissipation on the piezoresistance. The temperature-related bending component is based on the Euler-Bernoulli theory of elastic deformation applied to a multilayer cantilever. The heat dissipation component is based on energy conservation per unit time for a piezoresistive cantilever in a Wheatstone bridge circuit, representing a balance between electrical power input and heat dissipation into the environment. Conduction and convection are found to be the primary mechanisms of heat transfer, and the dependence of these effects on the thermal conductivity, temperature, and flow rate of the gaseous environment is described. The thermal boundary layer value which defines the length scale of the heat dissipation phenomenon is treated as an empirical fitting parameter. Using the model, it is found that the cantilever heat dissipation is unaffected by the presence of a thin polymer coating, therefore the residual thermal drift in the differential response of a coated and uncoated cantilever is the result of non-identical temperature-related bending. Differential response data shows that residual drift is eliminated under isothermal laboratory conditions but not the unregulated and variable conditions that exist in the outdoor environment (i.e., the field).

The two-component model is then validated by simulating the thermal drifts of an uncoated and a coated piezoresistive cantilever under field conditions over a 24 hour period using only meteorological data as input.

Keywords: Gas detection; Cantilever sensor; Piezoresistive; Thermal drift; Bimorph effect; Heat dissipation; Thermal conductivity

I. INTRODUCTION

Micro-electro-mechanical systems (MEMS) sensor arrays based on piezoresistive microcantilevers have been widely applied to chemical vapor and gas detection, where the embedded signal transducer (the piezoresistor) provides a more rugged, compact, and low-power alternative to the optical feedback method most commonly used in atomic force microscopy (AFM).¹⁻⁹ As detectors of the vapors of liquid chemicals^{1,2,5,6} or the sublimates of solids^{4,7}, piezoresistive cantilevers are coated with materials that have some chemical affinity for the gas-phase species of interest (i.e., the analyte). The chemical interaction between the analyte and sensing material (e.g., polymer) creates a bending response and a strain-induced piezoresistive change in the cantilevers, which is typically measured with a Wheatstone bridge circuit.

In addition to the piezoresistive changes created by the analyte/sensing material interaction are those resulting from thermal drift. The processes underlying thermal drift, if not identified and compensated for, will lead to erroneous sensor responses (e.g., false positive identification). The thermal drift in cantilever piezoresistance is primarily caused by two effects: 1) bending due to the different thermal expansion properties of the material layers within the cantilever, which varies with the temperature of the cantilever (i.e., the “bimorph effect”); 2) heat

dissipation by the electrically powered piezoresistor, which varies with the temperature and thermal conductivity of the environment. In the first effect, the temperature-related bending causes a change in resistance due to the strain sensitivity of the piezoresistor. The varying heat dissipation of the second effect also manifests itself as a change in resistance, in this case due to the functional dependence on piezoresistor temperature.

The typical compensation scheme for thermal drift is to operate the chemical vapor sensor with both coated (sensing) and uncoated (reference) cantilevers.¹⁰⁻¹² In this scheme, the thermal effects are assumed to be identical for the two types of cantilevers, so that subtraction of the piezoresistive changes in the uncoated cantilever from its coated counterpart yields a differential signal containing only the actual analyte response. More recently, it has been recognized that this differential signal will exhibit residual drift if the sensing and reference cantilevers experience different temperatures resulting from spatial temperature gradients, for example; such “real world” effects have thus spurred the development of piezoresistive cantilever designs with integrated temperature compensation.^{13,14} These designs are based on embedding a pair of strain-sensitive (piezoresistive) and strain-insensitive resistors in proximity within a single cantilever, where the latter type functions as a reference resistor in a Wheatstone bridge. This strategy is highly effective at eliminating thermal drift due to varying heat dissipation;^{13,14} since the piezoresistive and reference resistors experience the same local thermal environment and hence the same temperature-induced resistance fluctuations, the drift is cancelled out in the potential difference across the bridge between the resistors. However, this strategy does not compensate for the thermal drift due to temperature-related bending. Since a sensor coating will generally have a different thermal expansion coefficient than the cantilever, the degree of bending will be non-identical between the coated and reference cantilevers, and a

residual drift will be observed in the differential signal as the temperature conditions change. Therefore, successful thermal drift compensation schemes for piezoresistive cantilever sensors must simultaneously address the effects of heat dissipation and temperature-related bending.

The thermal drift in piezoresistive cantilevers has been examined experimentally by Thaysen *et al.* and the heat dissipation and bending effects separately fitted with simple linear models.¹⁰ In addition, the thermal drift phenomenon has been modeled by Li and Li using the finite element method, also revealing a linear piezoresistance change with changes in temperature.⁶ A detailed investigation of thermal conduction by a heated cantilever in air, also using finite element simulations, was conducted by Kim and King.¹⁵ However, a comprehensive analysis of the thermal drift exhibited by piezoresistive cantilevers, culminating in a closed-form expression for the response behavior derived from fundamental physical principles, has not been presented in the literature.

In an effort to understand the physical origins of thermal drift in piezoresistive cantilevers, a two-component thermal response model has been developed that describes both the effects of temperature-related bending and heat dissipation on the piezoresistance. In the first component, the bending of both uncoated and coated cantilevers as a function of temperature is analytically assessed using the Euler-Bernoulli theory of elastic beam deformation. The second component describes how the thermal conductivity, temperature, and flow rate of the gaseous environment affect the dissipation of heat by the piezoresistor. The model describes the operation of a piezoresistive cantilever in a Wheatstone bridge circuit in accordance with the principles of energy conservation and heat transfer under laminar flow conditions. The thermal boundary layer value which defines the length scale of the heat dissipation phenomenon is treated as an empirical fitting parameter; these values were obtained from the experimental

responses of a cantilever sensor array to binary gas mixtures of Kr/N₂ and He/N₂. It will be shown that the thermal drift compensation scheme involving the differential response of coated and uncoated cantilevers works well under isothermal laboratory conditions, but poorly under the unregulated and variable conditions that exist in the outdoor environment (i.e., the field). Since a successful transition of sensor technologies from the laboratory to the field requires the ability to function under a wide variety of possible conditions, more realistic applications of the thermal response model must account for scenarios where the thermal conductivity, temperature, and flow rate may all vary simultaneously. Therefore, an analysis of field data from a piezoresistive cantilever sensor array is presented; these data were collected over a 24-hour period, during which time meteorological data (temperature, relative humidity, barometric pressure) were also measured. To illustrate the validity of the model, the thermal drift in the observed responses of an uncoated and a coated piezoresistive cantilever were accurately simulated using only the meteorological data as input.

II. EXPERIMENT

Although the thermal response model is derived from the principles of energy conservation and heat transfer, the thermal boundary layer value defined above is treated as an empirical fitting parameter. This quantity describes the length scale over which heat is transferred from the cantilever piezoresistor to its environment, and varies in magnitude with the thermal conductivity of the environment. To investigate this behavior, a series of gas exposure calibration experiments were performed by exposing a piezoresistive cantilever array sensor to various test gases; this data was then used to determine the thermal boundary layer values from the model (Section IIIB).

A detailed description of the sensor, which employs CantiChip4 piezoresistive microcantilever arrays (Cantion A/S, Aalborg, Denmark), can be found in Ref. 9. In this previous work, piezoresistive cantilevers with polymeric coatings were used for chemical vapor detection, including the chemical warfare agents VX and sulfur mustard. To model a wide range of possible gaseous environments, two gases (Kr and He) were selected for the calibration experiments based on their extreme values of thermal conductivity (9.43 and 151.3 mW/m·K, respectively, at 298 K).¹⁶ Binary mixtures of each gas, with N₂ as the common diluent, were utilized. These ultrahigh purity gases were purchased commercially from various sources: 1) He from Matheson Tri-Gas (Parsippany, NJ, USA); 2) Kr from Airco (Santa Clara, CA, USA); 3) N₂ from Air Liquide America (Houston, TX, USA). A custom gas mixing system was used to prepare the binary mixtures with N₂ (Fig. 1). Concentrations of each gas mixture between zero (pure N₂) and 100% (pure gas) were obtained by a simple two-channel mixing based on relative flow rates. Gas temperatures were measured by a K-type thermocouple inserted into the mixed gas flow approximately 15 cm upstream of the sensor intake. Total flow rates between 18 and 90 standard cubic centimeters per minute (sccm) were measured downstream of the sensor exhaust outlet using an ADM2000 flow meter from Agilent Technologies (Santa Clara, CA, USA). All experiments were conducted under ambient conditions. The piezoresistance signals from eight cantilever channels were measured simultaneously during exposure to the test gases and then averaged. A schematic diagram of the sensor circuit is shown in Fig. 1.

To describe fully the thermal drift contribution due to varying heat dissipation, the resistance as a function of piezoresistor temperature must be explicitly determined. Thus, a resistance vs. temperature calibration was performed using IR microscopy. The cantilever temperature was increased by changing the applied bias voltage from 0 to 1.25 V while

simultaneously measuring the steady state blackbody infrared (IR) emission using a Merlin Laboratory camera (Indigo Systems, Santa Barbara, CA, USA). A stand-alone power supply was used to provide the voltage, since the sensor circuit operates at a fixed source bias ($V_s = 2.5$ V). The cantilever piezoresistance value was then calculated from the applied bias and measured current. The non-contact detection of mid-wave IR radiation was achieved using a liquid nitrogen cooled InSb camera capable of detecting radiation within the 3 to 5.5 μm wavelength range. The InSb camera uses a 320 \times 256 element focal plane array with 30 μm square pixels. Thermal background from the surroundings was removed with a 5.3 μm centered bandpass filter included as part of the cold shield and installed in front of the focal plane array. The manufacturer supplied Ge lens was used to focus the IR emission collected at normal incidence onto a detector providing ~ 6 $\mu\text{m}/\text{pixel}$ resolution. The analog output of the focal plane array is converted into 12-bit digital output from the camera, and the raw pixel counts of the captured thermal images were processed using the Mathematica software package (Wolfram Research, Champaign, IL, USA). The InSb camera was run at a maximum speed of 60 frames per second, and the linearity of the incident flux vs. counts was verified from room temperature (293 K) up to 1473 K using a blackbody source; this wide calibration range encompasses the typical operational temperature range (293-320 K) of the piezoresistive cantilevers in the Wheatstone bridge circuit. The correlation of IR flux with cantilever temperature requires the emissivity and absorption length of the cantilever materials (primarily low stress silicon nitride, SiN_x) at the measured wavelength, as well as a simultaneous temperature measurement. Since these properties are unknown, the thermal emission was calibrated using a 400 nm thick SiN_x membrane (Ted Pella, Redding, CA, USA) to approximate the cantilever; the membrane was used as a more mechanically robust substitute for the cantilever, which is too fragile for a direct

contact temperature measurement. The membrane was uniformly heated with a thermoelectric Peltier heater and the temperature slowly adjusted up to 333 K, while the steady state temperature was measured with a K-type thermocouple by careful contact with the membrane. A thermal image was recorded for each temperature reached by the membrane, which was later used to convert the pixel counts to estimated cantilever temperature values. However, in order to scale the measured IR emission from the 400 nm thick membrane to the ~500 nm thick cantilever, the normal emittance ε was approximated by $\varepsilon \approx \alpha t$,¹⁷ where α is the spectral absorption coefficient, and t represents the membrane or cantilever thickness. The pixel counts were then simply scaled according to the membrane to cantilever thickness ratio, which is a good approximation for thin nanometer scale layers.¹⁷ The final result of these measurements is a correlation of resistance with temperature for the piezoresistive cantilever.

Test data, obtained outside the laboratory under ambient conditions, were used to validate the thermal response model. The data were obtained over a 24 hour period (March 10 – 11, 2008) at a remote location in the hills of southwestern San Joaquin County, California, USA. In addition to measuring the piezoresistive changes of the cantilevers, the atmospheric conditions in the field were simultaneously monitored with an A-86403-00 weather station from the Cole-Parmer Instrument Company (Vernon Hills, IL, USA). This sensor suite recorded several types of meteorological data as a function of time: temperature, relative humidity, dew point, barometric pressure, wind speed and direction, and rain fall. The weather data were obtained at a selected rate of 16.7 mHz and the cantilever differential response data, obtained at a rate of 10 Hz, were downsampled to match the weather data rate. The piezoresistive cantilever sensor, fully enclosed in a plastic resin case, was vertically mounted on the weather station to minimize direct wind flux into the intake. In addition, an internal pump was used to draw air into the gas

flow cell at a constant flow rate of 8 standard cubic centimeters per minute (sccm). These measures (sensor orientation, pump) helped to eliminate the effect of the changing wind conditions on the piezoresistive cantilevers.

III. THERMAL RESPONSE MODEL

A. Temperature-Related Bending Component

The temperature-related bending of uncoated and coated cantilevers is first examined. The piezoresistive cantilevers used in this work are based on designs described in Ref. 18; the trimorphic structure is shown in Fig. 2, with a boron-doped amorphous silicon (a-Si) layer sandwiched between layers of SiN_x . Since these two materials have different coefficients of thermal expansion α , and the layers are assumed to be well adhered, any change in cantilever temperature T_c will induce a strain that manifests itself as a net bending. A general model for the uniform bending of a multilayer cantilever has been derived by Garcia and Lobontiu from the Euler-Bernoulli theory of elastic beam deformation.¹⁹ The key descriptor of bending is the radius of curvature R which, for a cantilever with n layers, is given by

$$R = \frac{\sum_{i=1}^n [E_i I_i - C_i (z_N - z_i)]}{\sum_{i=1}^n D_i (z_N - z_i)} \quad (1)$$

where E_i and I_i are the Young's modulus and second moment of area of the i^{th} layer, respectively. The positions of the symmetry axis of the i^{th} layer (z_i) and the zero-strain neutral axis of the composite cantilever (z_N) are measured from an origin set at the bottom of the cantilever, and defined as

$$z_i = \frac{t_i}{2} + \sum_{j=i+1}^n t_j \quad (2)$$

$$z_N = \frac{\sum_{i=1}^n z_i E_i A_i}{\sum_{i=1}^n E_i A_i} \quad (3)$$

The coefficients C_i and D_i for the i^{th} layer are expressed terms of its modulus, strain ε_i , thickness t_i , and cross-sectional area A_i :

$$C_i = \frac{E_i A_i}{2} \left\{ t_1 + 2 \sum_{k=2}^{i-1} t_k + t_i - \frac{\sum_{j=2}^n [E_j A_j (t_1 + 2 \sum_{k=2}^{j-1} t_k + t_j)]}{E_1 A_1 + \sum_{j=2}^n E_j A_j} \right\} \quad (4)$$

$$D_i = E_i A_i \left\{ \varepsilon_1 - \varepsilon_i - \frac{\sum_{j=2}^n [(\varepsilon_1 - \varepsilon_j) E_j A_j]}{E_1 A_1 + \sum_{j=2}^n E_j A_j} \right\} \quad (5)$$

The deflection δ of the cantilever tip can be simply obtained from R :

$$\delta = \frac{L^2}{2R} \quad (6)$$

where L is the cantilever length. The temperature-related bending creates a resistance change ΔR_c due to the strain dependence of the piezoresistor, and it is these changes in R_c that are a source of thermal drift in the differential response of piezoresistive cantilevers. The physical deflection and corresponding piezoresistance change can be related by the expression¹⁰

$$\frac{\Delta R_c}{R_c} = \left(K \frac{3t}{4L^2} \right) \delta \quad (7)$$

which holds for cantilevers with total thickness t , piezoresistor gauge factor K , and piezoresistor length equal to L . The i^{th} layer experiences a strain due to a change in temperature ΔT_c of the form

$$\varepsilon_i = \alpha_i \Delta T_c \quad (8)$$

where α_i is the coefficient of thermal expansion (K^{-1}). The thermal drift due to temperature-related bending, expressed as $\Delta R_c/R_c$, can thus be computed using Eqs. 1–8.

Next, the magnitude of the bending $\Delta R_c/R_c$ is estimated for uncoated and coated cantilevers. The temperature change ΔT that a sensor in the outdoor ambient environment encounters may exceed ± 20 K (see, for example, meteorological data compiled in Ref. 20); consequently, the powered piezoresistive cantilever will undergo an equivalent temperature change ΔT_c under these conditions. This can be simply understood in terms of the efficiency of heat transfer, which is determined by the gradient $T_c - T$. For example, if the environmental temperature rises, the magnitude of the gradient decreases and the rate of heat transfer to the environment is reduced; assuming constant power input, the result is a proportional rise in the cantilever temperature until a steady state is again attained. Using a representative value of $\Delta T = \Delta T_c = 20$ K and assuming that each material layer experiences the same temperature change, the $\Delta R_c/R_c$ values were computed for an uncoated cantilever, and a cantilever with a 100 nm thick glassy polyolefin coating using Eqs. 1–8. The modeled coating thickness is consistent with AFM measurements of polyolefin films deposited on SiN_x substrates by the same solvent casting method used to create the cantilever coatings.⁹ Since the chemical vapor sensor employs a variety of polymer coatings, $\alpha = 1.4 \times 10^{-4} \text{ K}^{-1}$ was used as a representative value; this value corresponds to a glassy polystyrene film on an oxidized silicon substrate.²¹ The α for a-Si ($\sim 2.8 \times 10^{-6} \text{ K}^{-1}$) and SiN_x ($\sim 3.7 \times 10^{-6} \text{ K}^{-1}$) thin films were estimated from the literature,^{22,23} as were the Young's moduli for polystyrene ($\sim 3.5\text{--}4$ GPa), a-Si (~ 130 GPa), and SiN_x (~ 240 GPa) thin films.²⁴⁻²⁶ A piezoresistor gauge factor $K = 17$ is representative of the a-Si cantilevers used in this study.¹⁸ The results show a bending-related thermal drift of $\Delta R_c/R_c = 7.3 \times 10^{-5}$ and -2.6×10^{-4} for uncoated and coated cantilevers (respectively) subjected to $\Delta T_c = 20$ K.

To determine the relative significance of this drift, a direct comparison can be made to an actual detection response. Using data from the study described in Ref. 9 as an example, a

cantilever coated with poly(α -methylstyrene) (PMS) and exposed to 90 parts-per-million (ppm) of distilled sulfur mustard (bis(2-chloroethyl) sulfide, HD) in dry air at 296 K produces a response $\Delta R_c/R_c = -7.1 \times 10^{-5}$, which is 28% of the thermal drift magnitude for $\Delta T_c = 20$ K. The analyte response corresponds to a swelling of the polymer coating with HD sorption, which leads to bending. It is evident that the temperature- and analyte-related bending may often be comparable in magnitude during the variable temperature conditions of typical field operations. Therefore, bending-related thermal drift must be generally included in treatments of the piezoresistive cantilever response behavior.

B. Heat Dissipation Component

In this section, the heat dissipation component of the thermal response model is addressed. As the gaseous environment becomes more or less conductive to heat, the piezoresistor decreases or increases its temperature, respectively, under constant electrical power; thermal drift results from the functional dependence of the piezoresistance on temperature. Thus, changes in the piezoresistance are related to changes in the thermal properties of the environment, which must be accounted for in order to describe properly the thermal drift due to varying heat dissipation. The transfer of electrical energy from the piezoresistor as heat generally depends on the thermal conductivity, temperature, and gaseous flow rate of its surroundings. Several possible mechanisms of heat dissipation must be considered to account fully for the thermal response of the cantilever: 1) direct heat conduction into the gas and cantilever substrate, as described by the Fourier law; 2) heat transfer into the gas attributed to both free (buoyancy driven) and forced (flow driven) convection, also described by the Fourier law; 3) radiative heat transfer into the gas and cantilever substrate, as described by

the Stefan-Boltzmann law. Under general conditions where the cantilever is surrounded by gas at finite pressures (e.g., 1 torr and greater) and non-zero flow rates, both conduction and convection must be considered. Radiative heat dissipation will be examined in Section IIIC; using the results of the gas exposure calibration experiments discussed below, it will be shown that these contributions are negligible.

The conservation of energy per unit time for the piezoresistor is expressed as

$$\frac{(\Delta V_c)^2}{R_c} = \frac{T_c - T}{R_t} \quad (9)$$

where ΔV_c is the voltage drop across the piezoresistance R_c , T_c and T are the piezoresistor and environmental temperatures (respectively), and R_t represents the total thermal resistance of the gas and cantilever substrate due to conduction and convection. The temperature gradient $T_c - T$ occurs over finite distances into the gas and the cantilever substrate; this distance defines the thermal boundary layer ℓ over which the heat transfer occurs. The left-hand side of Eq. 9 represents the electrical power delivered to the piezoresistor, while the right-hand side represents the rate of its heat dissipation into the environment described by the Fourier law. Using the well-known voltage divider relation for ΔV_c , Eq. 9 is solved to obtain an expression for the total thermal resistance:

$$R_t = \left(\frac{T_c - T}{R_c} \right) \left(\frac{R_1 + R_c}{V_s} \right)^2 \quad (10)$$

where the circuit parameters R_1 and V_s are defined in Fig. 1. The thermal response of the piezoresistor is most practically described by changes in R_c , since this is what the Wheatstone bridge circuit measures; therefore, Eq. 10 must be solved for R_c . However, two complications arise: 1) R_c is a function of T_c , and this relation must be explicitly determined; 2) the effects of

conduction and convection contained within R_t must be modeled using the properties of the environment surrounding the piezoresistor.

To resolve these complications, the dependence of R_c on T_c is first addressed. The R_c vs. T_c calibration was performed on an uncoated cantilever using IR microscopy. Representative temperature maps at applied biases of 0.0 and 1.25 volts, along with a corresponding photomicrograph, are shown in Fig. 3. Although the piezoresistive layer extends over the full length of the cantilever, only the free (unclamped) end experiences any visible heating above the ambient temperature. By comparing the images in Fig. 3, it is evident that the heated region ($\sim 35 \mu\text{m}$ long) encompasses only that portion of the current-carrying path in the immediate vicinity of the 180° bend. The presence of “hot spots” due to non-uniform Joule heating is consistent with current crowding, a phenomenon in integrated circuits that occurs wherever localized variations in resistivity exist (e.g., flip chip solder joints,²⁷ interconnect vias and contacts,²⁸ and serpentine film resistors²⁹). This localized effect is enhanced by the relatively insulated condition of the cantilever free end in the gaseous environment compared to the base region connected directly to the massive silicon substrate, which acts as a heat sink. The “cool” portions of the piezoresistor between the 180° bend and the cantilever base remain near room temperature due to strong heat conduction into the high heat capacity substrate.

Since the heated region of the cantilever is sharply confined, T_c is defined as the effective temperature for the piezoresistor equal to the arithmetic average over all the pixels within this region. A plot of the cantilever resistance R_c vs. relative temperature $T_c - T_0$, with reference temperature $T_0 = 293 \text{ K}$, is shown in Fig. 4. Since the temperature dependence of R_c appears to be fairly linear, a least-squares fit corresponding to the equation

$$R_c(T_c) = [\alpha_r R_c(T_c = T_0)](T_c - T_0) + R_c(T_c = T_0) \quad (11)$$

is applied to the calibration data, yielding a temperature coefficient of resistance $\alpha_r = 2.86 \times 10^{-3} \text{ K}^{-1}$.

This value of α_r is obtained under the assumption that the increase in measured resistance with increasing T_c is due entirely to the intrinsic temperature dependence of R_c . However, as the applied bias and hence supplied power increases, the temperature relative to the zero-bias “off” state also increases. This increasing temperature difference leads to a proportionate bending of the cantilever from its off state, such that the measured R_c values also include the thermal drift effects discussed in Section IIIA. The temperature change that occurs between the 0 V and 1.25 V biased conditions of the IR calibration is calculated at $\Delta T_c = 13 \text{ K}$ using Eq. 11. Applying Eqs. 1–8 for an uncoated cantilever, the bending-related thermal drift is found to be $\Delta R_c/R_c = 4.8 \times 10^{-5}$. With a nominal value of $R_c = 4000 \text{ } \Omega$, the maximum drift contribution is $\sim 0.2 \text{ } \Omega$ and decreases to zero in the off state. If these corrections are applied to the measured resistance values, the resulting change in α_r is less than 0.5%. Consequently, the thermal drift due to varying heat dissipation is effectively decoupled from the bending-related thermal drift, which supports the independent treatment of these effects in Sections IIIB and IIIA, respectively.

Since Eq. 9 addresses the energy conservation per unit time of the heated cantilever, the delivery of electrical energy to that portion of the piezoresistor for which $(T_c - T_0) > 0$ must be accounted. Taking a nominal current path down the geometric center of the rectangular cross section piezoresistor, and assuming a semi-circular path around the 180° bend, the heated segment is determined to be $\sim 28\%$ of the total resistive path. Since the off state resistance $R_c(T_0)$ at reference temperature $T_0 = 293 \text{ K}$ is readily calculated from Eq. 11, subtracting the contribution $(1-0.28)R_c(T_0)$ from R_c yields the resistance from only the heated segment. Therefore, if only the electrical power delivered to the heated piezoresistive segment is

considered, which subsequently dissipates heat into its surroundings, then Eq. 10 must be slightly modified to obtain

$$R_t = \left[\frac{T_c - T}{R_c - 0.72R_c(T_0)} \right] \left(\frac{R_1 + R_c}{V_s} \right)^2 \quad (12)$$

The functional dependence of R_t on the conductive and convective heat dissipation mechanisms is now described. A purely theoretical expression for R_t due to conduction and convection is obtained by considering the structure and operation of the piezoresistive cantilever. The a-Si layer forms a thin slab of heated material encapsulated by SiN_x (Fig. 2). In addition, the resistance vs. temperature calibration revealed that only the free end portion of the resistor, ~35 μm in length, becomes appreciably heated above T during sensor operation (Fig. 3). Given the Cartesian symmetry of the heated piezoresistor segment at T_c , the total R_t can be considered equivalent to six one-dimensional (1-D) heat transfer channels. The 1-D channels simultaneously dissipate heat through each face of the heated slab due to the gradient $T_c - T$; consequently, their thermal resistances must add inversely in the same fashion as a parallel network of electrical resistors with a common applied bias. A schematic representation of the functionally equivalent thermal resistor network is shown in Fig. 5. Although the piezoresistive portion of the a-Si slab is U-shaped, the heated segment is treated as a uniform, orthorhombic shape for simplicity. For the top, bottom, free end, and sides of the heated a-Si slab, the heat must pass first through the SiN_x layer (ℓ_{SiN}) and then the gas thermal boundary layer (ℓ_{gas}); for these 1-D channels, the serial layer resistances are directly summed.

Conduction and convection (free and forced) serve as simultaneous heat dissipation mechanisms, and their relative contribution can be assessed by the Nusselt number (Nu). This quantity is defined as the ratio of convective to conductive heat loss, and can be expressed in

terms of the convective heat transfer coefficient h and the thermal conductivity k : $Nu = h\ell/k$.³⁰ The gas flow conditions in the vicinity of the cantilever determine the magnitude of the convective losses. In the current flow cell geometry, the gas flows perpendicularly to the cantilever length L and parallel to its horizontally-oriented surface (Fig. 1). Since the cantilever is very thin compared to its lateral dimensions (Fig. 2), and streamline flow is assumed over its leading edge, the top and bottom surfaces should be most affected by convective heat transport. The thermal resistances of these two surfaces dominate the gas-dependent behavior of R_t due to the reciprocal summation of the parallel dissipation paths; this preponderant influence is attributed to their relatively large surface areas, which lead directly to correspondingly small thermal resistances. Therefore, the Nusselt number should be incorporated into the thermal resistance expressions for the top and bottom surfaces.

From the Fourier law, the thermal resistance associated with conduction in a material of thermal conductivity k is theoretically represented as ℓ/kA ; in this expression, A is the heated surface area. Similarly, the thermal resistance due to convection is $1/hA$, where h is the flow-dependent heat transfer coefficient. Using these expressions, the thermal resistance of the top surface is given by

$$\frac{1}{R_{top,gas}} = \left[\frac{\ell_{gas}}{k_{gas}(L_h W_{Si})} \right]^{-1} + \left[\frac{1}{h_{gas}(L_h W_{Si})} \right]^{-1} \quad (13)$$

where L_h is the length of the heated region ($\sim 35 \mu\text{m}$) and W_{Si} is the width of the a-Si slab. Solving for $R_{top,gas}$, and using the definition of Nu , the total thermal resistance of the flowing gas is

$$R_{top,gas} = \frac{\ell_{gas}}{k_{gas}(L_h W_{Si})} (Nu + 1)^{-1} \quad (14)$$

and the total thermal resistance R_{top} through the SiN_x and gas is given by

$$R_{top} = \frac{\ell_{SiN,top}}{k_{SiN}(L_h W_{Si})} + \frac{\ell_{gas}}{k_{gas}(L_h W_{Si})} (Nu + 1)^{-1} \quad (15)$$

A similar expression holds for the total thermal resistance of the bottom cantilever surface. Without the convective contributions, the thermal resistances associated with the free end and sides are

$$R_{end} = \frac{1}{W_{Si} t_{Si}} \left(\frac{\ell_{SiN}}{k_{SiN}} + \frac{\ell_{gas}}{k_{gas}} \right) \quad (16)$$

$$R_{side} = \frac{1}{L_h t_{Si}} \left(\frac{\ell_{SiN}}{k_{SiN}} + \frac{\ell_{gas}}{k_{gas}} \right) \quad (17)$$

where t_{Si} is the thickness of the a-Si layer. The 1-D thermal resistance associated with heat transport from the heated region through the base of the cantilever and into the substrate, is simply given as

$$R_{sub} = \frac{\ell_{Si}}{k_{Si}(W_{Si} t_{Si})} \quad (18)$$

The total thermal resistance R_t is then trivially computed using Eqs. 15–18:

$$\frac{1}{R_t} = \frac{1}{R_{top}} + \frac{1}{R_{bot}} + \frac{1}{R_{end}} + \frac{2}{R_{side}} + \frac{1}{R_{sub}} \quad (19)$$

Examining the expressions for the 1-D thermal resistances, it is evident that the value of nearly every variable can found in the literature or determined from the sensor design specifications; however, quantification of the thermal boundary layers into the gas and the cantilever substrate (ℓ_{gas} and ℓ_{Si} , respectively) is less obvious. The following scenarios provide some insight into these quantities: under fixed flow and ambient temperature conditions, the arrival of a relatively insulating gas (i.e., decreased k_{gas}) will cause T_c to increase but ℓ_{gas} to shrink; in the limit of a

perfect thermal insulator (i.e., vacuum), ℓ_{gas} will approach zero. Alternatively, the introduction of flow to a stagnant gas would facilitate heat dissipation, creating the same effect as introducing a more conductive gas; thus, T_c will decrease (cooling) but ℓ_{gas} will expand.

For ℓ_{Si} , a value of $\sim 12 \mu\text{m}$ was inferred from the IR micrographs of the resistance vs. temperature calibration (Fig. 3); the sharp spatial temperature gradient at the edge of the heated piezoresistor segment was reconciled with the pixel resolution of $6 \mu\text{m}$ by assuming a drop of $T_c - T$ over a maximum of two adjoining pixels. In the presence of gas flow, ℓ_{Si} should increase by a factor of $(Nu+1)$.

To explore the correlation between k_{gas} and ℓ_{gas} , calibration experiments were performed by exposing uncoated piezoresistive cantilevers to various Kr/N₂ and He/N₂ mixtures and measuring the ΔR_c thermal responses with respect to a pure N₂ reference. For these exposure data, the bending-related thermal drift can be computed using Eqs. 1–8, with the ΔT_c obtained by direct substitution of the measured R_c into Eq. 11. The maximum values of ΔT_c occur with exposure to pure Kr (+8.5 K) and pure He (-10.0 K), with corresponding drifts of $\Delta R_c/R_c = 3.1 \times 10^{-5}$ and -3.7×10^{-5} , respectively. In comparison, since the piezoresistance has a high sensitivity to ΔT_c ($\sim 11 \Omega/\text{K}$, Fig. 4), the gas exposure response has considerably larger values of $\Delta R_c/R_c = 2.4 \times 10^{-2}$ (Kr) and -2.8×10^{-2} (He). Thus, bending-related thermal drift has a negligible effect on the gas exposure data, and the entirety of the measured response can be attributed to changes in the thermal conductivity of the gas.

These experimental data, along with the R_c vs. T_c calibration (Eq. 11) and known circuit parameters, were used to calculate R_t from Eq. 12. Similarly, R_t was determined from Eq. 19 up to the unknown ℓ_{gas} , where the k_{gas} and Nu values were estimated for each test mixture (see EPAPS supplementary material at [AIP URL]). By combining these expressions for R_t , the ℓ_{gas}

value is obtained for each binary mixture examined; these results are plotted as a function of k_{gas} (Fig. 6). A linear dependence was observed, with a least squares fit

$$\ell_{gas} = 420.05k_{gas} + 5.8197 \quad (20)$$

where ℓ_{gas} and k_{gas} are given in units of μm and $\text{W/m}\cdot\text{K}$, respectively. The gas thermal boundary layer exhibits the expected trend of decreasing value with decreasing thermal conductivity. Since the isothermal contours around the cantilever become increasingly distorted with increasing flow, as demonstrated in a prior finite element modeling study,³¹ the assumed symmetry of a singular ℓ_{gas} value represents an average value. The ℓ_{gas} values, of the same magnitude as the cantilever dimensions, are also consistent with the previous work.³¹

With ℓ_{gas} described by the empirical expression of Eq. 20, the thermal resistance R_t of the environment surrounding the piezoresistor can be entirely predicted from Eqs. 15–19 using only: 1) the thermal conductivity of the gaseous environment; 2) the external and internal dimensions of the cantilever structure and; 3) the operating flow conditions which determine the Nusselt number. Using the thermal resistance, along with the R_c vs. T_c calibration (Eq. 11), Eq. 12 can now be solved to provide an explicit expression of the piezoresistance R_c in terms of the thermal properties of the environment. Solving Eq. 11 for T_c produces the expression:

$$T_c = \left(T_0 - \frac{1}{\alpha_r} \right) + \left[\frac{1}{\alpha_r R_c (T_0)} \right] R_c \quad (21)$$

Denoting the first and second bracketed quantities as ξ_1 and ξ_2 , respectively, this expression is substituted into Eq. 12 and simplified to the final result:

$$R_c^3 + aR_c^2 + bR_c + c = 0 \quad (22)$$

where the multiplicative constants a through c are defined:

$$a = \frac{\xi_1 - T + 2R_1\xi_2}{\xi_2} \quad (23)$$

$$b = \frac{R_1^2\xi_2 + 2R_1(\xi_1 - T) - R_tV_s^2}{\xi_2} \quad (24)$$

$$c = \frac{R_1^2(\xi_1 - T) + 0.72R_tV_s^2R_c(T_0)}{\xi_2} \quad (25)$$

Cardano's method can be used to solve the cubic equation in R_c ,³² yielding a single real root that represents the predicted cantilever resistance. Equations 22–25 can be used to evaluate the thermal drift due to varying heat dissipation, much as Eqs. 1–8 were used to evaluate the thermal drift due to temperature-related bending in Section IIIA. Together, these sets of equations constitute the thermal response model for piezoresistive cantilevers in closed form.

The bending-related thermal drift, as formulated in the previous section, depends on the cantilever temperature change ΔT_c (Eq. 8). However, any fluctuations in T_c are ultimately the result of variations in the heat dissipation mechanism due to: 1) variations in the environmental temperature T and/or; 2) variations in the thermal resistance R_t , which depends essentially on the thermal conductivity of the gaseous environment. Therefore, although the bending and heat dissipation effects were independently formulated in Sections IIIA and IIIB, respectively, these two components of the thermal response model are functionally linked through the common variable T_c . The estimation of the bending-related drift in Section IIIA required the piezoresistor temperature change ΔT_c corresponding to $\Delta T = 20$ K. It was assumed, by a simple physical argument, that ΔT_c would rise (heat) or fall (cool) in equal proportion to fluctuations in ΔT : $\Delta T_c = \Delta T$. By substituting appropriate values for T and $T + 20$ K into Eqs. 23–25, Eq. 22 can be solved for R_c at each temperature; then, the resistance values can be translated into T_c values using Eq. 21. For a typical piezoresistive cantilever used in this work, the resulting ΔT_c is calculated to be

20 K. Thus, fluctuations in the piezoresistor temperature T_c have a simple and direct relation to fluctuations in the environmental temperature T .

One noteworthy observation is that a virtually identical ΔT_c value is obtained for either uncoated or coated cantilevers in cases where the gas thermal conductivity changes. This can be traced to the thermal resistance of the polymer coated cantilever surface, which can be expressed as

$$R_{top} = \frac{\ell_{SiN,top}}{k_{SiN}(L_h W_{Si})} + \frac{\ell_p}{k_p(L_h W_{Si})} + \frac{\ell_{gas}}{k_{gas}(L_h W_{Si})} (Nu + 1)^{-1} \quad (26)$$

and includes the serial resistances of the SiN_x and polymer layers (denoted by subscript “p”), and the gaseous environment (cf. Eq. 15). The polymer is assumed to have a uniform thickness ℓ_p and cover the entire top surface of the cantilever including the heated area $L_h W_{Si} = 1.7 \times 10^{-9} \text{ m}^2$. A thermal conductivity $k_p = 0.16 \text{ W/m}\cdot\text{K}$, corresponding to a poly(methylmethacrylate) thin film on Si, is used as a representative value.^{33,34} A value $Nu = 2.44$ corresponds to a Reynolds number $Re = 9.4 \times 10^{-2}$ and gas flow rate 2 cm/s over the cantilever, which are typical operating values for the gas sensor (see EPAPS supplementary material at [AIP URL]). For a polymer coating of 100 nm thickness, Eq. 26 yields individual thermal resistance values of 15 K/W (SiN_x), 358 K/W (polymer), and $1.3 \times 10^5 \text{ K/W}$ (gas). Since the gas will always have a thermal conductivity that is 1–3 orders of magnitude smaller than either the cantilever or coating materials, it will always dominate the heat dissipation mechanism, and the coating will have no meaningful insulative or conductive effect on the cantilever.

The preceding analysis also reveals the role that the coating plays in the non-identical thermal drift behavior of uncoated (reference) vs. coated (sensing) cantilevers. This issue, first considered in the introduction, describes the residual drift in the differential signal between the cantilevers. Since the coating thermal resistance is relatively insignificant compared to the gas,

its presence does not alter the cantilever heat dissipation and therefore cannot be a source of residual thermal drift. Nevertheless, such residual drift is evident in differential field data which will be presented in Section IV. Thus, ruling out the heat dissipation drift mechanism leads to the conclusion that temperature-related bending (Section IIIA) is the principal source of the residual drift. As was shown in that section, the degree of bending $\Delta R_c/R_c$ induced by $\Delta T = 20$ K was non-identical for uncoated (7.3×10^{-5}) and coated (-2.6×10^{-4}) cantilevers, leading directly to the observed residual thermal drift. This calculation presumed that both cantilevers experience the same change in environmental temperature; certainly, as indicated in Refs. 13 and 14, the existence of an actual temperature difference between the cantilevers would also give rise to non-identical $\Delta R_c/R_c$ values.

As a final comment, we note that the argument presented above applies only to *residual* thermal drift – i.e., there is no *difference* in heat dissipation between uncoated and coated cantilevers. However, the thermal drift for an *individual* cantilever due to varying heat dissipation is of considerable magnitude due to the highly sensitive dependence of R_c on ΔT_c . For example, substituting $\Delta T_c = \Delta T = 20$ K into Eq. 11 yields $\Delta R_c/R_c = 5.7 \times 10^{-2}$. Therefore, when considering the signal of an individual piezoresistive cantilever rather than the differential signal, the heat dissipation mechanism must be identified as the principal source of thermal drift.

C. Radiative heat dissipation

The heat dissipation component of the thermal model is based on the conservation of energy per unit time for the piezoresistor (Eq. 9). It was assumed that thermal radiation was not a significant heat dissipation mechanism compared to conduction and convection, and its associated power loss term was omitted from Eq. 9. To justify this omission, two requirements

must be satisfied: 1) the radiated power is negligibly small compared to the electrical power input, implying that conduction and convection are the primary methods of heat dissipation; 2) the fluctuations in radiated power with changes in T_c are negligibly small compared to the associated fluctuations in electrical power created by phenomena of interest (e.g., an analyte detection event). The second statement calls for an analysis similar to the one performed at the end of Section IIIA. In the previous case, it was shown that temperature-related bending could create a response of comparable magnitude to one created by the detection of a gas-phase analyte, thus requiring the inclusion of the bending-related drift response in the model. Here, the radiated power changes will be shown to be insignificant compared to the power changes created by introducing a low thermal conductivity gas (Kr), as well as those associated with an analyte detection event.

To address the first requirement, the net radiated power P_r from a cantilever is estimated using the Stefan-Boltzmann law, where the total heated surface area $A = 3.5 \times 10^{-9} \text{ m}^2$ and the proportionality constant σ is $5.67 \times 10^{-8} \text{ W/m}^2\text{K}^4$:

$$\begin{aligned} P_r &= A\varepsilon\sigma(T_c^4 - T^4) \\ &= (3.5 \times 10^{-9} \text{ m}^2)(0.1)(5.67 \times 10^{-8} \text{ W/m}^2\text{K}^4)[(317 \text{ K})^4 - (293 \text{ K})^4] = 54 \text{ nW} \end{aligned} \quad (27)$$

In the absence of IR absorbance data for SiN_x at the measured wavelength ($5.3 \text{ }\mu\text{m}$), the absorption length for the semi-transparent cantilever is estimated as $\sim 5 \text{ }\mu\text{m}$ with a corresponding emissivity $\varepsilon = 0.1$,³⁵ this estimate is consistent with a previously measured emissivity value of ~ 0.2 obtained for a thin film $\text{SiO}_2\text{-Si}_3\text{N}_4$ sandwich with thickness comparable to the cantilever.³⁶ The temperature $T_c = 317 \text{ K}$ of the heated piezoresistor segment corresponds to pure Kr exposure as observed in the calibration experiments, while $T = 293 \text{ K}$ represents a typical ambient

temperature. In comparison, the electrical power input to the heated piezoresistor segment under these conditions is

$$P_e = \frac{(\Delta V_c)^2}{R_c(317 \text{ K}) - 0.72R_c(T_0)} = \frac{(1.22 \text{ V})^2}{4110.6 \Omega - 0.72(3846.9 \Omega)} = 1.1 \text{ mW} \quad (28)$$

where Eq. 11 was used to compute R_c at $T_c = 317 \text{ K}$. Since the radiated power is an exceedingly small fraction of the electrical power input, the initial assumption of exclusively conductive and convective heat dissipation is proved correct.

Next, the second requirement is addressed by examining two phenomena of interest related to sensor operations, and comparing their corresponding responses to the accompanying radiated power change. In the first scenario, a representative cantilever exposed to N_2 is then exposed to Kr, a gas of lower thermal conductivity (25.8 vs. 9.43 mW/m·K at 298 K, respectively).¹⁶ The measured resistance values of 4020.8 Ω (N_2) and 4113.2 Ω (Kr) can be substituted into Eq. 21 to obtain the corresponding T_c values of 308.8 K and 317.2 K, respectively. The resulting change in electrical power P_e during Kr exposure is

$$|\Delta P_e| = (\Delta V_c)^2 \left| \frac{1}{R_{c,Kr}} - \frac{1}{R_{c,N_2}} \right| = (1.22 \text{ V})^2 \left| \frac{1}{4113.2 \Omega} - \frac{1}{4020.8 \Omega} \right| = 8.3 \mu\text{W} \quad (29)$$

Using the Stefan-Boltzmann law, the change in net radiated power during Kr exposure is

$$\begin{aligned} \Delta P_r &= A\varepsilon\sigma(T_{c,Kr}^4 - T_{c,N_2}^4) \\ &= (3.5 \times 10^{-9} \text{ m}^2)(0.1)(5.67 \times 10^{-8} \text{ W/m}^2\text{K}^4) \left[(317.2 \text{ K})^4 - (308.8 \text{ K})^4 \right] = 20.5 \text{ nW} \end{aligned} \quad (30)$$

The variation in radiated power is $\sim 0.2\%$ of the power change occurring during Kr exposure, supporting the omission of thermal radiation in the model. In a second scenario, the example exposure of a PMS-coated cantilever to 90 ppm of HD at 296 K (Section IIIA) is revisited. With a measured resistance value of 4094.1 Ω at this temperature, exposure to the analyte causes a

fractional resistance change of -7.1×10^{-5} such that $R_c = 4093.8 \Omega$ at the peak of HD exposure.

The associated power change is

$$|\Delta P_e| = (\Delta V_c)^2 \left| \frac{1}{R_{c,HD}} - \frac{1}{R_{c,N_2}} \right| = (1.22 \text{ V})^2 \left| \frac{1}{4093.8 \Omega} - \frac{1}{4094.1 \Omega} \right| = 26.6 \text{ nW} \quad (31)$$

In this case, where the response is created by analyte-induced swelling strain in the polymer coating, the cantilever temperature T_c will change only if the k and/or T values of the environment change. The previously examined case of Kr exposure practically represents a worst-case scenario for a change in k (only Xe has a lower thermal conductivity amongst gases).¹⁶ In the hypothetical event that a Kr exposure occurs simultaneously to a 90 ppm HD exposure, the radiated power change will be $\sim 77\%$ of the analyte-induced bending signal. An identical effect will also occur if $\Delta T = 317.2 \text{ K} - 308.8 \text{ K} = 8.4 \text{ K}$ occurs during the HD exposure time, such that $\Delta T_c = 8.4 \text{ K}$ also results. Such a change in the environmental temperature is unlikely under passive heating conditions during the time to peak exposure, which is typically seconds to minutes; this assessment, while typically true under ambient field conditions, may not be true under artificial circumstances (e.g., industrial process conditions). Therefore, provided that such unlikely events do not occur during the field-based sensing of an analyte and alter ΔT_c , the radiated power change will be relatively minimal. As a final comment, it is evident that in the limit of small analyte-induced responses, such as those that occur for trace airborne concentrations, even small fluctuations in temperature will create radiative signal contributions of comparable magnitude; in such applications, Eq. 9 must be explicitly reformulated to include radiated power.

IV. SIMULATION OF FIELD DATA USING THE THERMAL RESPONSE MODEL

The impact of thermal drift on piezoresistive cantilever response is now examined under both isothermal laboratory conditions and the varying conditions that are present in the field. The use of a reference cantilever to obtain a differential signal from a chemically functionalized cantilever is highly effective at compensating for minor thermal drift, particularly under constant or near constant temperature conditions such as those present in a climate controlled laboratory. Under these conditions and in the absence of gas-phase analytes, the differential signal is constant such that its slope with respect to time is essentially zero. As an example, Fig. 7 shows the differential signals vs. time for two piezoresistive cantilevers coated with PMS and poly(vinyl chloride-*co*-vinyl acetate-*co*-2-hydroxypropyl acrylate) (PVC). Before exposure to acetonitrile at an airborne concentration of 6.7 parts per thousand at $\sim 21^{\circ}\text{C}$, the differential signals are constant to within ± 2 mV over a 1.9 hour period; the stability against thermal drift was assessed by comparing this variation to the 1 mV peak-to-peak noise, and the peak differential responses of 1081 mV (PMS) and 275 mV (PVC) to the analyte.

Differential data obtained in the field under outdoor conditions, where temperatures vary significantly throughout the day, exhibit obvious thermal drift (Fig. 8). The differential signal, corresponding to a PMS-coated cantilever, exhibits a variation that follows the ambient temperature trend and attains a maximum amplitude of ~ 255 mV (Fig. 8a). In contrast, two test exposures to methylene chloride, puff discharged from the headspace of a wash bottle, are less than 188 mV in magnitude (Fig. 8b). According to the two-component thermal model developed in Section III and the discussion at the end of Section IIIB, the residual thermal drift in the differential signal is the result of temperature-related bending, while the drift in each cantilever is

dominated by the heat dissipation mechanism. Since PMS exhibits hydrophobic characteristics due to the phenyl pendant group, bending contributions from the absorption of ambient water vapor should be minimal.

To verify that the observed drift is consistent with the thermal model, the nature of the gaseous environment must be considered. The ambient air is approximated as a binary mixture of water vapor and N_2 of varying concentration; this is a reasonable assumption since: 1) air is over 99% N_2 and O_2 by volume;¹⁶ 2) the thermal conductivities of N_2 and O_2 are nearly identical (e.g., 25.2 and 25.8 mW/m·K, respectively);¹⁶ 3) argon, the third largest constituent at 0.934% by volume in dry air, is constant in concentration;³⁷ 4) water vapor is present at about 1% concentration (50% humidity, 20°C) and varies with the weather conditions.

Under this assumption, the piezoresistance R_c as a function of time t for uncoated and coated cantilevers was separately computed from the two-component thermal model (Eqs. 1–8, 22–25) using the meteorological data (T , relative humidity, barometric pressure) as the only variable input. First, the contributions from the heat dissipation component (Section IIIB) were computed. The air thermal conductivity k_{air} was computed from the temperature dependent values of the pure components (N_2 and H_2O) using the relative humidity RH (%) and barometric pressure to determine the mixing parameters (see Supplementary Material). Then, the thermal boundary layer value ℓ_{air} was computed from k_{air} (Eq. 20). The Nusselt number was calculated as described in the supplementary material; however, the water vapor viscosity μ_{H_2O} (Pa·s) and specific heat capacity c_{p,H_2O} (J/kg·K) were instead computed by empirical fits taken from Ref. 38 for humid air:

$$\mu_{H_2O} = (4.000 \times 10^{-7})T - 2.869 \times 10^{-5} \quad (32)$$

$$c_{p,H_2O} = (1.941 \times 10^{-2})T^2 - (1.086 \times 10^1)T + 3.388 \times 10^3 \quad (33)$$

The thermal resistance R_t of the air was then computed from Eqs. 15–19 using k_{air} , ℓ_{air} , Nu , and the external and internal dimensions of the cantilever structure. Finally, the R_c contributions from the heat dissipation component were calculated from Eqs. 22–25 at each time step using R_t and the circuit component values (Fig. 1); for convenience, the R_c values were translated into the corresponding Wheatstone bridge voltages V_b at a gain of 1000x.

A brief but noteworthy digression involves the model values of R_t . The computed values for the total effective thermal resistance – for example, 8.3×10^4 K/W for air at $RH = 52$, $T = 293$ K, and $Re = 0-0.1$ – can be directly compared to values computed by Kim and King using continuum finite element (FE) simulations for thermal conduction between a heated cantilever and a quiescent air environment.¹⁵ For a total heated surface area $A = 3.5 \times 10^{-9}$ m², R_t can be alternately expressed as a heat transfer coefficient with value ~ 3450 W/m²·K; this compares favorably to the FE-derived value (~ 7000 W/m²·K), particularly considering the simplified assumptions of cantilever and thermal boundary layer geometry used in the present study (Section IIIB).

Second, the bending contributions (Section IIIA) to the piezoresistance were computed using Eqs. 1–8. The temperature of the heated piezoresistor segment T_c was computed at each time step from the previously calculated R_c values using Eq. 21; then, using the initial recorded temperature (293.0 K) as the reference temperature, the resulting ΔT_c values were substituted into Eq. 8, and the R_c contributions from temperature-related bending were computed using Eq. 7. All of the thermomechanical parameters described in Section IIIA were used in the calculations. These values were finally combined with the heat dissipation R_c values to produce the simulated piezoresistance value at each time step of the weather data acquisition.

The thermal model simulations of V_b vs. t can be directly compared to the measured signal for both uncoated and coated cantilevers; this is shown in Fig. 9, along with the T and RH data for comparison. The largest discrepancy between the simulated and observed data occurs during the late morning and early afternoon of 3/11/2008. Except for this period of several hours, the thermal drift trends in the simulated V_b closely follow those observed in the experimental data and are remarkably coincident during the overnight hours. There is a small difference between the uncoated and coated cantilever signals, seen in Fig. 9b, which is due non-identical temperature-related bending (Section IIIB). To test the fidelity of the simulated drift corrections, the calculated trends are subtracted from the experimental data for both cantilever types. The individual corrected signals from each cantilever are then subtracted from one another to give a corrected differential signal (Fig. 9c). The corrected differential response, corresponding to the PMS-coated cantilever, exhibits a maximum drift amplitude of ~ 42 mV, a 6-fold decrease from the raw observed signal.

A reconstruction of the experimental conditions, based on the local terrain of the test site and the solar position during the sampling period, yielded several facts: 1) the waning afternoon light shined on the sensor until $\sim 5:45$ pm, with sunset following at 7:09pm; 2) the discrepancy between the simulated and observed data began after $\sim 9:20$ am, which marked the onset of direct sunlight exposure on the sensor; 3) the discrepancy peaks near midday, and begins to decrease again as the afternoon progresses. These foregoing observations support a localized heating phenomenon: the sensor enclosure likely provided an insulating effect around the flow cell and cantilevers, slightly enhancing the local temperature compared to that measured by the exposed temperature sensor of the weather station. In the absence of sunlight, the insulative effect disappeared as thermal equilibration occurred between the air within and without the sensor case.

To illustrate this effect, a correction for enhanced local temperatures was introduced into the model. Since the most significant discrepancies between the simulated and observed data occurred between about 9:50am to 3:05 pm, coinciding with the period of greatest illumination intensity, a variable multiplicative factor for T was used in this time interval. To model the expected local warming and cooling trends as the sun passed over the sensor, the factor was increased linearly from 1.00 to 1.08 (9:50am – 12:10am), then held constant at 1.08 (12:10am – 1:50pm), and finally decreased linearly from 1.08 to 1.00 (1:50pm – 3:05pm). At peak warming, the 8% correction is equivalent to a local enhancement of +5°C over the measured T . The model simulation for an uncoated cantilever, with the locally enhanced T values, is shown in Fig. 10; the simulated trend closely follows the experimental data, in support of the localized heating supposition. Overall, the match between the simulated and observed behavior of a piezoresistive cantilever in a Wheatstone bridge circuit validates the thermal response model developed in this work. The correspondence between the simulated and observed response is marred only by the occurrence of intermittent artifacts in the experimental data. Since these artifacts do not simultaneously appear in the meteorological data and hence the derived simulation, they must originate from the experimental sensor apparatus itself. We speculate that these artifacts result from local heating effects on the electronics, which are also housed in the same resin case as the cantilever sensor array.

The foregoing correction for enhanced local temperature implies that collocation of the T sensor with the cantilevers should eliminate the discrepancy between the simulated and observed data. This strategy should also eliminate the residual fluctuations seen in the corrected differential signal (Fig. 9c), which are most likely the result of the localized internal heating from the cantilevers as described in this work. Such local heating, albeit minor due to the low power

consumption of the sensor, would create a persistent discrepancy in the environmental temperature between the sensor interior and exterior that is only partially alleviated by the forced convection mode of gas sampling.

V. CONCLUSIONS

A closed-form model has been developed which can account for the thermal drift of a piezoresistive microcantilever sensor employing a Wheatstone bridge circuit. The two-component model describes both the effects of temperature-related bending and heat dissipation on the piezoresistance. The temperature-related bending component is based on the Euler-Bernoulli theory of elastic deformation applied to a multilayer cantilever, and expresses the net bending that occurs when the layers are subjected to a thermally induced strain. The heat dissipation component is based on the conservation of energy per unit time, representing a balance between electrical power input and heat dissipation into the environment. The cantilever heat dissipation is unaffected by the presence of a polymer coating and therefore the residual thermal drift in the differential response of a coated and uncoated cantilever is the result of non-identical temperature-related bending.

The thermal response model has been used to simulate successfully the thermal drift of an uncoated and a coated cantilever under outdoor conditions over a 24 hour period using only meteorological data as input. One application for the model is in software implemented compensation schemes for thermal drift, provided accurate measurements of the gas temperature near the cantilever are made simultaneously. Another potential application is the use of a piezoresistive cantilever as a gas sensor, exploiting physical rather than chemical means (e.g., functional coatings) for detection. Since the thermal conductivity of the gaseous environment

depends on its composition, the model can be used to predict either the thermal response to various gas analytes or, more importantly, as a means of deducing the gas identity.

ACKNOWLEDGEMENTS

This work was performed under the auspices of the U.S. Department of Energy by Lawrence Livermore National Laboratory under Contract DE-AC52-07NA27344. The authors would like to thank J. L. Herberg for contributions to this work.

REFERENCES

- ¹T. L. Porter, M. P. Eastman, D. L. Pace, and M. Bradley, *Sens. Actuator A* **88**, 47-51 (2001).
- ²N. Abedinov, C. Popov, Z. Yordanov, T. Gotszalk, P. Grabiec, W. Kulisch, I. W. Rangelow, D. Filenko, and Y. Shirshov, *J. Vac. Sci. Technol. B* **21**, 2931-2936 (2003).
- ³A. Kooser, R. L. Gunter, W. D. Delinger, T. L. Porter, and M. P. Eastman, *Sens. Actuators B* **99**, 474-479 (2004).
- ⁴L. A. Pinnaduwege, D. L. Hedden, A. Gehl, V. I. Boiadjiev, J. E. Hawk, R. H. Farahi, T. Thundat, E. J. Houser, S. Stepnowski, R. A. McGill, L. Deel, and R. T. Lareau, *Rev. Sci. Instrum.* **75**, 4554-4557 (2004).
- ⁵G. M. Zuo, X. X. Li, P. Li, T. T. Yang, Y. L. Wang, Z. X. Cheng, and S. L. Feng, *Anal. Chim. Acta* **580**, 123-127 (2006).
- ⁶P. Li and X. X. Li, *J. Micromech. Microeng.* **16**, 2539-2546 (2006).
- ⁷G. M. Zuo, X. X. Li, P. Li, Y. L. Wang, Z. X. Cheng, and S. L. Feng, in *5th IEEE Sensors Conference; Vol. 1-3* (IEEE, Daegu, South Korea, 2006), p. 749-752.

- ⁸T. L. Porter, T. L. Vail, M. P. Eastman, R. Stewart, J. Reed, R. Venedam, and W. Delinger, *Sens. Actuator B* **123**, 313-317 (2007).
- ⁹A. Loui, T. V. Ratto, T. S. Wilson, S. K. McCall, E. V. Mukerjee, and B. R. Hart, *Analyst* **133**, 608-615 (2008).
- ¹⁰J. Thaysen, A. Boisen, O. Hansen, and S. Bouwstra, *Sens. Actuators A* **83**, 47-53 (2000).
- ¹¹N. V. Lavrik, M. J. Sepaniak, and P. G. Datskos, *Rev. Sci. Instrum.* **75**, 2229-2253 (2004).
- ¹²L. A. Pinnaduwege, H. F. Ji, and T. Thundat, *IEEE Sens. J.* **5**, 774-785 (2005).
- ¹³B. W. Chui, L. Aeschimann, T. Akiyama, U. Staufer, N. F. d. Rooij, J. Lee, F. Goericke, W. P. King, and P. Vettiger, *Rev. Sci. Instrum.* **78**, 043706 (2007).
- ¹⁴F. Goericke, J. Lee, and W. P. King, *Sens. Actuators A* **143**, 181-190 (2008).
- ¹⁵K. J. Kim and W. P. King, *Appl. Therm. Eng.* **29**, 1631-1641 (2009).
- ¹⁶*CRC Handbook of Chemistry and Physics; Vol.*, edited by D. R. Lide (CRC Press, Boca Raton, FL, 2005).
- ¹⁷D. C. Harris, *Infrared Phys. Technol.* **39**, 185-201 (1998).
- ¹⁸X. Yu, J. Thaysen, O. Hansen, and A. Boisen, *J. Appl. Phys.* **92**, 6296-6301 (2002).
- ¹⁹E. Garcia and N. Lobontiu, *Smart Mater. Struct.* **13**, 725-732 (2004).
- ²⁰J. E. Ephrath, J. Goudriaan, and A. Marani, *Agric. Syst.* **51**, 377-393 (1996).
- ²¹D. J. Pochan, E. K. Lin, S. K. Satija, and W. L. Wu, *Macromolecules* **34**, 3041-3045 (2001).
- ²²J. Fabian and P. B. Allen, *Phys. Rev. Lett.* **79**, 1885-1888 (1997).
- ²³M. Maeda and K. Ikeda, *J. Appl. Phys.* **83**, 3865-3870 (1998).
- ²⁴Y. X. Ren and D. C. C. Lam, *Mater. Sci. Eng. A-Struct. Mater. Prop. Microstruct. Process.* **467**, 93-96 (2007).
- ²⁵X. X. Li, T. Ono, Y. L. Wang, and M. Esashi, *Appl. Phys. Lett.* **83**, 3081-3083 (2003).

- ²⁶C. M. Stafford, B. D. Vogt, C. Harrison, D. Julthongpiput, and R. Huang, *Macromolecules* **39**, 5095-5099 (2006).
- ²⁷J. W. Nah, J. O. Suh, K. N. Tu, S. W. Yoon, V. S. Rao, V. Kripesh, and F. Hua, *J. Appl. Phys.* **100**, 5 (2006).
- ²⁸J. T. Trattles, A. G. Oneill, and B. C. Mecrow, *IEEE Trans. Electron Devices* **40**, 1344-1347 (1993).
- ²⁹F. M. Barlage, *IEEE Trans. Parts, Hybrids, Packag.* **9**, 262-263 (1973).
- ³⁰F. P. Incropera, D. P. DeWitt, T. L. Bergman, and A. S. Lavine, *Introduction to Heat Transfer*, 5th ed. (John Wiley & Sons, Inc., Hoboken, NJ, 2007).
- ³¹M. M. Yovanovich and P. Teertstra, *J. Thermophys. Heat Transf.* **15**, 205-211 (2001).
- ³²U. K. Deiters, *AIChE J.* **48**, 882-886 (2002).
- ³³S. Govorkov, W. Ruderman, M. W. Horn, R. B. Goodman, and M. Rothschild, *Rev. Sci. Instrum.* **68**, 3828-3834 (1997).
- ³⁴D. C. Chu, M. Touzelbaev, K. E. Goodson, S. Babin, and R. F. Pease, *J. Vac. Sci. Technol. B* **19**, 2874-2877 (2001).
- ³⁵R. Gardon, *J. Am. Ceram. Soc.* **39**, 278-287 (1956).
- ³⁶F. Völklein, *Thin Solid Films* **188**, 27-33 (1990).
- ³⁷S. C. Hwang, R. D. Lein, and D. A. Morgan, in *Kirk-Othmer Encyclopedia of Chemical Technology; Vol. 17* (John Wiley & Sons, 2005), p. 343-383.
- ³⁸P. T. Tsilingiris, *Energy Conv. Manag.* **49**, 1098-1110 (2008).

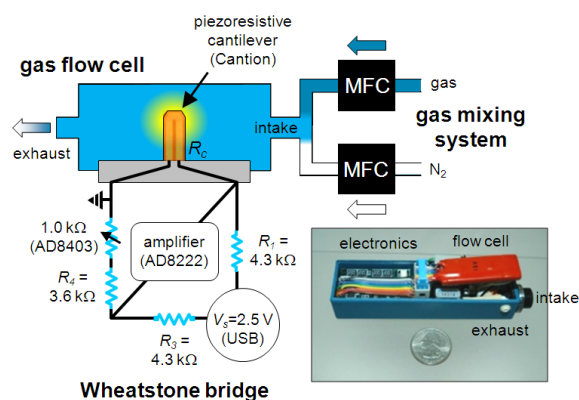


FIG. 1. Schematic overview of the experimental apparatus, including the gas sensor (Wheatstone circuit, gas flow cell) and gas mixing system; only one of the eight cantilevers and corresponding bridge circuits is represented for clarity. Inset: Photograph of the gas sensor, with protective case removed, next to a US quarter.

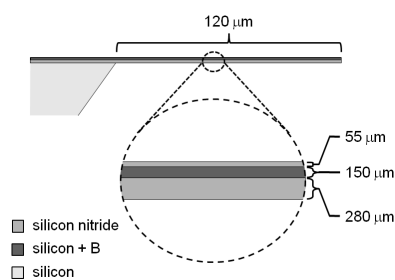


FIG. 2. Schematic cross section of a piezoresistive cantilever (internal dimensions taken from Ref. 18).

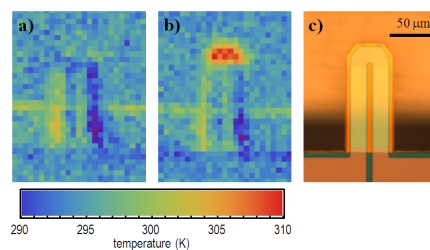


FIG. 3. (a) and (b) IR images of a piezoresistive cantilever at 0.0 and 1.25 volts, respectively. (c) photomicrograph of cantilever. All images are shown at the same relative scale.

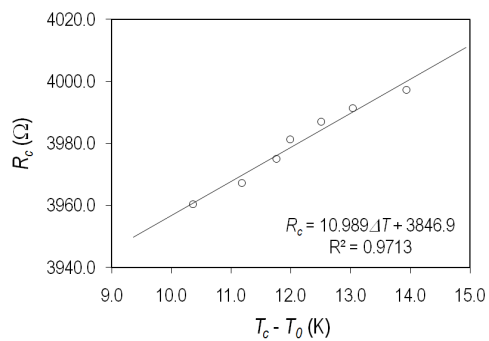


FIG. 4. Plot of piezoresistance R_c vs. relative temperature $T_c - T_0$ data from the IR calibration. The least squares regression line is shown.

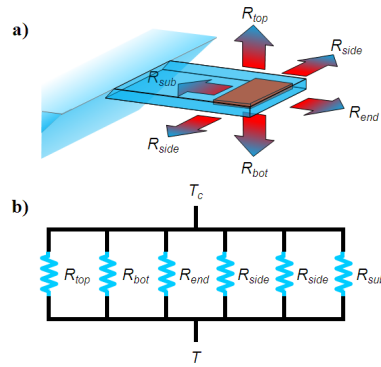


FIG. 5. (a) Schematic diagram of a cantilever, with six 1-D heat transfer channels for the heated piezoresistive segment. (b) The functionally equivalent thermal resistor network.

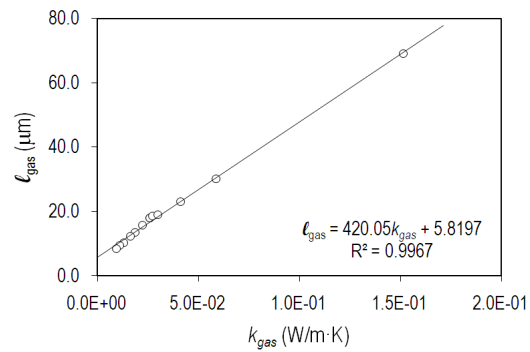


FIG. 6. Plot of optimized l_{gas} values vs. thermal conductivity k_{gas} for the Kr/ N_2 and He/ N_2 experimental mixtures. The least squares regression line is shown.

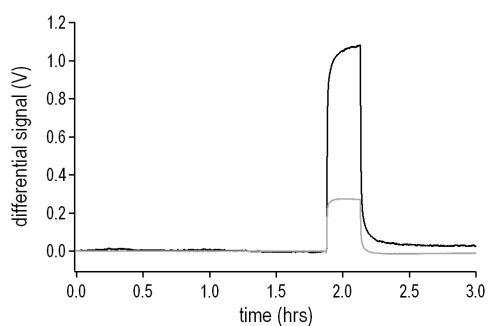


FIG. 7. Plot of differential signal vs. time for two cantilevers coated with poly(α -methylstyrene) (PMS, black line) and poly(vinyl chloride-*co*-vinyl acetate-*co*-2-hydroxypropyl acrylate) (PVC, gray line). An exposure to 6.7 parts per thousand of acetonitrile in dry air at 21°C is initiated at 1.87 hrs and turned off at 2.13 hrs.

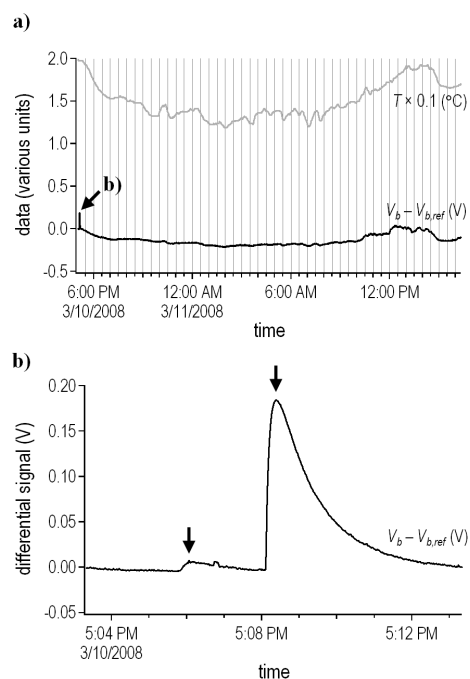


FIG. 8. a) Plot of differential signal $V_b - V_{b,ref}$ vs. time for a PMS-coated cantilever. The scaled temperature $T(\times 0.1)$ vs. time is also shown for comparison. b) Two test exposures to methylene chloride vapor (arrows) at the outset of the experiment.

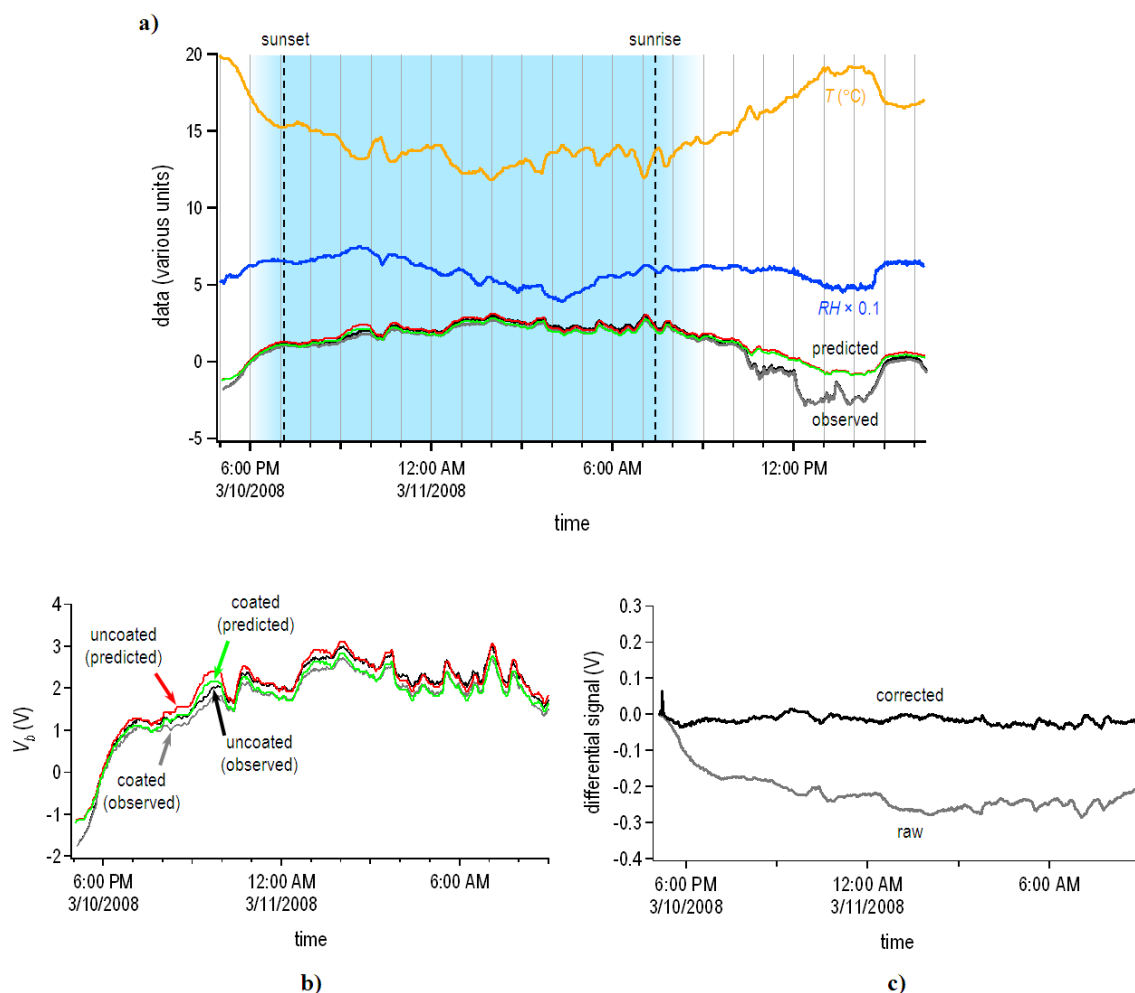


FIG. 9. (a) Plot of simulated and observed bridge voltages V_b vs. time for an uncoated and PMS-coated cantilever. The temperature T and scaled relative humidity RH ($\times 0.1$) are shown for comparison. (b) Close-up of the plot in part a), showing the simulated and observed cantilever signals between 5:00 pm (3/10/2008) and 9:00 am (3/11/2009). (c) Differential signals (PMS-coated minus uncoated) corresponding to part (b) with (“corrected”) and without (“raw”) the simulated drift correction (cf. Fig. 8).

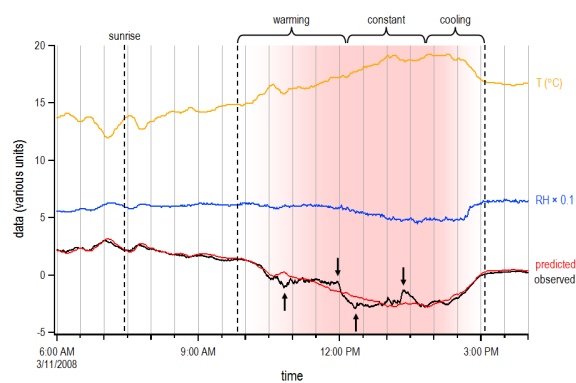


FIG. 10. Plot of simulated and observed bridge voltages V_b vs. time for an uncoated cantilever. The simulated response includes a correction for enhanced local temperatures during the period of greatest illumination intensity (cf. Fig. 9a). Artifacts in the observed data are indicated (arrows). The temperature T and scaled relative humidity RH ($\times 0.1$) are shown for comparison.